TABLE I. The total Compton cross sections $d\sigma/d\Omega$ in electron units for Li and Ge in the Waller-Hartree theory, the Bonham corrections δ_1 [Eq. (20)] and δ_2 [Eq. (21)] to the Waller-Hartree theory (Mo $K\alpha$), and the total cross section obtained from an integration of the Compton profiles in the impulse approximation.

$\frac{\sin\theta}{\lambda}$	Li $\lvert E_0\rvert = 202$ eV		Ge $\lvert E_0\rvert = 56\,400$ eV			
	WH	Impulse	WH	δ_1	δ_2	Impulse
0	0	0	0	0	0.073	0
0.1	1.05	1.00	1.59	−0.02	0.075	5.72
0.2	1.44	1.47	4.73	−0.074	0.08	9.05
0.3	1.82	1.96	7.34	−0.15	0.08	11.2
0.4	2.16	2.32	9.91	−0.24	0.10	13.1
0.5	2.42	2.54	12.3	−0.34	0.12	14.7
0.6	2.60	2.66	14.4	−0.44	0.15	16.2
0.7	2.70	2.73	16.0	−0.53	0.19	17.5
0.9	2.76	2.76	18.5	−0.75	0.30	18.4
1.1	2.74	2.73	20.2	−0.98	0.46	20.4
		$\lvert\delta_1\rvert < 0.03$				
		$\lvert\delta_2\rvert < 0.02$				

Bonham corrections to the Waller-Hartree theory.

As can be seen in Table I, the difference between the Waller-Hartree theory even with the corrections by Bonham can be large [for example, at $(\sin\theta)/\lambda = 0.1$ Å^{-1} for Ge]. It is obviously desirable to have measurements to evaluate the two theories. A more complete set of tables of total Compton cross sections are available from one of the authors (R. J. W.).

IV. CONCLUSION

The most important point suggested by our results is that the impulse approximation for core electrons provides a convenient scheme for subtracting their contributions from the observed Compton profiles. Since the valence electron contribution is only sizable near the Compton peak, the error in separating the valence electron profile from the core can probably be kept to a few percent.

The total cross sections as calculated in the Waller-Hartree approximation and the impulse approximation can differ greatly but not at the large values of $(\sin\theta)/\lambda$ employed in Compton profile measurements. Thus, absolute normalization of the profiles can be done to within a few percent when conditions are chosen such that $(\sin\theta)/\lambda > 1.0$ Å^{-1}.

ACKNOWLEDGMENT

The authors wish to thank Dr. A. Kugler, Dr. P. Kleban, and Dr. D. Weick for useful discussions and Mrs. Athena Harvey for her help with the computational work.

*Work performed while a postdoctoral fellow at Army Materials and Mechanics Research Center, Watertown, Mass.

[1]W. C. Phillips and R. J. Weiss, Phys. Rev. 111, 790 (1968).

[2]R. J. Weiss and W. C. Phillips, Phys. Rev. 176, 900 (1968).

[3]P. Eisenberger and P. Platzman, Phys. Rev. A 2, 415 (1970).

[4]P. Eisenberger, Phys. Rev. A 2, 1678 (1970).

[5]I. Waller and D. R. Hartree, Proc. Roy. Soc. (London) A124, 119 (1929).

[6]R. A. Bonham, J. Chem. Phys. 43, 1460 (1965).

[7]R. Currat, P. D. DeCicco, and R. Kaplow, Phys. Rev. B 3, 243 (1971).

[8]W. A. Rachinger, J. Sci. Instr. 25, 254 (1948).

[9]W. C. Phillips and R. J. Weiss, Phys. Rev. 171, 790 (1968).

[10]R. J. Weiss, A. Harvey, and W. C. Phillips, Phil. Mag. 17, 241 (1968).

PHYSICAL REVIEW B VOLUME 4, NUMBER 12 15 DECEMBER 1971

Self-Consistent Electronic Structure of Titanium. II†*

R. M. Welch‡ and E. H. Hygh
Department of Physics, University of Utah, Salt Lake City, Utah 84112
(Received 23 July 1971)

The band structure, Fermi surface, and density of states from an augmented-plane-wave calculation of titanium are presented and compared with previously reported results. The present calculation differs from the earlier work in that the potential is a self-consistent muffin-tin form and further in that the coefficient of the Slater exchange term is $\frac{3}{4}$ instead of 1.

I. INTRODUCTION

The aims of the present calculation are (i) to obtain the self-consistent-potential energy bands and Fermi surface of titanium within the muffin-tin one-electron potential-energy form[1] for comparison with a previous "one-shot" calculation,[2] (ii) to determine the effect on the self-consistent energy eigenvalues at the Γ point for various choices of the parameter α in the $\chi\alpha$-method[3] exchange poten-

tial, (iii) to predict de Haas–van Alphen periods for the conduction electrons in titanium, and (iv) to obtain a set of crystal wave functions which can be used as a starting set for determining a nonspherical "true" crystal potential for titanium.

The calculation is performed using the augmented-plane-wave (APW) method of Slater[4] since rapid convergence is obtained for the $3d$ transition metals using this method. Group theory is used to reduce the size of the secular determinant and self-consistency is acquired only with respect to a charge density determined by a sampling of 136 high-symmetry points in the Brillouin zone (BZ). In Sec. II, we describe how the self-consistent muffin-tin charge density and potential are determined, and we discuss the group theory for the nonsymmorphic space group of the hcp crystal structure. In Sec. III, we present energy convergence studies with respect to truncation of the angular momentum quantum number l which appears in the APW matrix elements and the iterated crystal charge density, and we present our reasons for iterating only the charge density produced by the original $3d^2 4s^2$ atomic states with all lower-energy charge densities being assumed "frozen." Next, we study the convergence of the self-consistent energy eigenvalues at the Γ point for three choices of α, $\alpha = 1$, $\frac{5}{6}$, and $\frac{3}{4}$, and we calculate the energy bands and Fermi surface for $\alpha = \frac{3}{4}$, a choice which produces the most physically reasonable results. Finally, we compute a density-of-states histogram for comparison with the experimental photoemission work of Eastman[5] and the density of states found by Compton scattering,[6] and we calculate an electron specific-heat coefficient to compare with the specific-heat measurements of Daunt[7] and Gschneider.[8]

In Sec. IV, we compare the present energy bands and Fermi surface with those obtained by the authors in a previous calculation,[2] hereafter referred to as HW (I). Also, where possible, we contrast this work with the results of Altmann and Bradley[9] (AB), which they obtained using a modified form of the cellular method suggested by Slater[10] and developed by Altmann.[11] Finally, we discuss possible orbital periods of conduction electrons for comparison with de Haas–van Alphen measurements of the Fermi surface. Since no experimental data are available, we compare these periods with those predicted in HW (I).

II. THEORETICAL ANALYSIS

A. APW Method

The APW method has been discussed at length in the literature. We review the method briefly and refer the reader elsewhere[12] for a more detailed discussion. The method yields the best solution to the one-electron Schrödinger equation for a crystal potential usually chosen to be of a muffin-tin form. This approximation to the true crystal potential is one in which a sphere (called an APW sphere) is constructed about each atomic site such that no overlapping of spheres occurs. The potential is assumed to be spherically symmetric within each APW sphere and to be constant in the region between spheres. The wave function is expanded in terms of products of radial functions and spherical harmonics inside each sphere and is represented by a Fourier series of plane waves in the region between spheres. The APW's thus have the form

$$\chi_{\vec{k}_g} = \sum_{l,m} A_{lm} R_l(\rho, E') Y_{lm}(\hat{\rho}) \quad \text{inside APW sphere}$$

$$= e^{i\vec{k}_g \cdot \vec{r}} = e^{i\vec{k}_g \cdot (\vec{r}_\nu + \vec{\rho})} \quad \text{outside} .$$

The radial function $R_l(\rho, E')$ satisfies the equation

$$-\frac{1}{\rho^2}\frac{d}{d\rho}\left(\rho^2 \frac{dR_l}{d\rho}\right) + \left(\frac{l(l+1)}{\rho^2} + V^{\text{in}}(\rho)\right) R_l = E' R_l , \tag{1}$$

where $V^{\text{in}}(\rho)$ is the spherically symmetric part of the muffin-tin potential. The coefficients A_{lm} are chosen to make the APW's continuous across the APW sphere boundary defined by radius S_ν. This requires that

$$A_{lm}(\vec{k}_g, E') = 4\pi e^{i\vec{k}_g \cdot \vec{r}_\nu} i^l Y^*_{lm}(\hat{k}_g) j_l(k_g S_\nu)/R_l(S_\nu, E') .$$

The wave vector $\vec{k}_g = \vec{k}_0 + \vec{g}$ determines the transformation properties of the eigenfunction being calculated. The component $\vec{k}_0$ is the reduced wave vector in the first BZ, and $\vec{g}$ is one of the set of reciprocal-lattice vectors for the crystal. The eigenfunction $\psi_{\vec{k}_g}$ is made up of all APW's which belong to the $\vec{k}_0$th representation. Hence, we have

$$\psi_{\vec{k}_g} = \psi_{\vec{k}_0} = \sum_{\vec{g}} C_{\vec{k}_0 + \vec{g}} \chi_{\vec{k}_0 + \vec{g}} , \tag{2}$$

where the expansion coefficients $C_{\vec{k}_0 + \vec{g}}$ are determined using the variational principle.

Schlosser and Marcus[13] have obtained an appropriate variational expression for E which is valid for wave functions exhibiting continuity in value but discontinuity in slope over a spherical surface,

$$E\int_{\Omega_{\text{I}} + \Omega_{\text{II}}} \psi^* \psi \, dV = \int_{\Omega_{\text{I}} + \Omega_{\text{II}}} \psi^* H \psi \, dV - \frac{1}{2}\int_{\text{sphere}} (\psi^*_{\text{II}} + \psi^*_{\text{I}}) \left(\frac{\partial \chi_{\text{II}}}{\partial \rho} - \frac{\partial \psi_{\text{I}}}{\partial \rho}\right) dS .$$

The surface term takes the discontinuity of slope into account. Ω_{I} is the volume within the APW spheres and Ω_{II} is the volume outside. Substituting (2) into this expression and minimizing E with re-

spect to the coefficients $C_{\vec{k}_0+\vec{g}}$ lead to a set of linear equations for each wave vector $\vec{k}_0$ as given by

$$\sum_{\vec{g}'} (H_{\vec{g}\vec{g}'} + S_{\vec{g}\vec{g}'} - E\Delta_{\vec{g}\vec{g}'}) C_{\vec{k}_0+\vec{g}'} = 0 \quad \text{for all } \vec{g} \ .$$

The eigenvalues E are found by solving the determinantal equation

$$\det \left| H_{\vec{g}\vec{g}'} + S_{\vec{g}\vec{g}'} - E\Delta_{\vec{g}\vec{g}'} \right| = 0 \ .$$

The matrix elements in the determinant are given by[12]

$$(H_{\vec{g}\vec{g}'} + S_{\vec{g}\vec{g}'} - E\Delta_{\vec{g}\vec{g}'}) = \Omega_{\text{cell}} (\vec{k}_g^2 - E)\, \delta_{\vec{g}\vec{g}'} - 4\pi \sum_\nu S_\nu^2 e^{i(\vec{g}-\vec{g}')\cdot\vec{r}_\nu} G^\nu_{\vec{g}\vec{g}'} \ , \qquad (3)$$

where

$$G^\nu_{\vec{g}\vec{g}'} = (\vec{k}_g \cdot \vec{k}_{g'} - E) \frac{j_1(|\vec{g}-\vec{g}'|S_\nu)}{|\vec{g}-\vec{g}'|} - \sum_{l=0}^{\infty} (2l+1) \times P_l(\vec{k}_g \cdot \vec{k}_{g'}) j_l(k_g S_\nu) j_l(k_{g'} S_\nu) \frac{R_l'(S_\nu, E)}{R_l(S_\nu, E)} \ . \qquad (4)$$

This form of the matrix elements is acquired by setting the trial energy E' equal to the eigenenergy E, thus eliminating the term in the matrix element depending on $E' - E$ (the term involving the portion of the integral extending throughout only the spherical regions). The APW functions and matrix elements depend implicitly on the eigenenergy in this procedure. One chooses values of E, computes the matrix elements, and then computes the determinant. When the proper values are acquired, the determinant vanishes.

For each eigenvalue computed, the corresponding expansion coefficients $C_{\vec{k}_0+\vec{g}}$ can be determined by a matrix inversion technique. The coefficients so determined yield an appropriate expansion for the eigenfunction given by (2) above.

B. Self-Consistent Muffin-Tin Potential

The starting point of an APW calculation is the determination of a muffin-tin potential. A method for constructing this form of crystal potential using atomic potentials obtained from Hartree-Fock-Slater self-consistent-field (SCF) calculations is described by Mattheiss.[14] Once the potential has been obtained, the electronic structure is calculated as described in Sec. II A. Using the eigenvalues from this calculation, a new crystal charge density is calculated using the expression

$$\rho(\vec{r}) = \sum_{\vec{k}_0} |\psi_{\vec{k}_0}|^2 = \sum_{\vec{k}_0} \sum_{\vec{g}\vec{g}'} C_{\vec{k}_0+\vec{g}} C_{\vec{k}_0+\vec{g}'} \chi^*_{\vec{k}_0+\vec{g}} \chi_{\vec{k}_0+\vec{g}'} \ ,$$

where the sum on $\vec{k}_0$ is over all occupied Bloch states. The potential for the next iteration is obtained by solving Poisson's equation (in atomic units)

$$\nabla^2 V(\vec{r}) = -8\pi\rho(\vec{r}) \ .$$

Within the muffin-tin approximation, the charge density is made up of two parts: There is the spherically averaged density inside the APW sphere given by

$$\bar{\rho}_{\text{in}}(r) = \frac{1}{4\pi} \int_{\vec{k}_0} \sum |\psi_{\text{in}}|^2 \sin\theta \, d\theta \, d\phi \ ,$$

with

$$\psi_{\text{in}}(r) = \sum_{\vec{g}} C_{\vec{k}_0+\vec{g}} \sum_{l,m} A_{lm} R_l(r) Y_{lm}(\theta, \phi), \quad r < S_\nu \ .$$

Using the expressions for the A_{lm}, the spherically averaged density can be written

$$\bar{\rho}_{\text{in}}(r) = \frac{1}{4\pi} \sum_{\vec{k}_0} \sum_{\vec{g}\vec{g}'} C^*_{\vec{k}_0+\vec{g}} C_{\vec{k}_0+\vec{g}'} \sum_l 4\pi \frac{R_l^2(r)}{R_l^2(S_\nu)} \times (2l+1) j_l(k_g S_\nu) j_l(k_{g'} S_\nu) P_l(\vec{k}_g \cdot \vec{k}_{g'}) \ . \qquad (5)$$

Next, there is the constant density in the region outside the APW spheres. This is given by the volume average over the region outside

$$\bar{\rho}_{\text{out}} = \frac{1}{\Omega_0} \int_{\Omega_0} \sum_{\vec{k}_0} |\psi_{\text{out}}|^2 r^2 dr \sin\theta \, d\theta \, d\phi \ ,$$

where Ω_0 is the volume of the region outside given by $\Omega_{\text{cell}} - \sum_\nu \frac{4}{3}\pi S_\nu^3$ and where

$$\psi_{\text{out}} = \sum_{\vec{g}} C_{\vec{k}_0+\vec{g}} e^{i(\vec{k}_0+\vec{g})\cdot\vec{r}} \ .$$

Carrying out the integration over the entire cell volume and then subtracting off the contribution of the sphere volume gives

$$\bar{\rho}_{\text{out}} = \frac{1}{\Omega_0} \sum_{\vec{k}_0} \sum_{\vec{g}\vec{g}'} C^*_{\vec{k}_0+\vec{g}} C_{\vec{k}_0+\vec{g}'} \times \left(\Omega_{\text{cell}} \delta_{\vec{g}\vec{g}'} - 4\pi \sum_\nu S_\nu^2 e^{i(\vec{g}-\vec{g}')\cdot\vec{r}_\nu} \frac{j_1(|\vec{g}-\vec{g}'|S_\nu)}{|\vec{g}-\vec{g}'|} \right) . \qquad (6)$$

The normalization integral for these averaged charge densities can now be performed. It is given by

$$N_0 = \bar{\rho}_{\text{out}} \Omega_0 + 4\pi \sum_\nu \int_0^{S_\nu} \bar{\rho}_{\text{in}}(r) r^2 dr \ .$$

Since there are two electrons for each Bloch state, N_0 can be chosen so that the state represents either one or two electrons per unit cell. Typically it is chosen to give one electron per unit cell, and the multiplication by two is performed later.

With $\bar{\rho}_{\text{in}}(r)$ and $\bar{\rho}_{\text{out}}$ determined as described, the problem of finding the potential is straightforward. Rudge[15] has given a complete development for the calculation of the Coulomb and exchange potential energies in the case of a crystalline potential energy of a general kind, i.e., one involving nonsphericity. His approach utilizes a decomposition of a crystalline charge density into three parts.

Three separate problems are then solved: (i) a Fourier series problem, (ii) a zero multiple-moment problem, and (iii) a generalized Ewald potential problem. Within the muffin-tin approximation the problems become extremely simple. The Fourier series problem involves only the $\vec{g}=0$ coefficient defined by $\rho(\vec{g}=0)=\bar{\rho}_{\text{out}}$. The zero multiple-moment problem involves only an array of monopoles and a spherical density, namely, $Z_\nu - Q$ and $\bar{\rho}_{\text{in}}(r)-\bar{\rho}_{\text{out}}$ where Q is chosen to give a zero monopole moment for each sphere,

$$Z_\nu - Q - \int_0^{S_\nu} [\rho_{\text{in}}(r)-\rho_{\text{out}}]\,4\pi r^2 dr = 0 \ . \tag{7}$$

Finally the generalized Ewald potential problem involves an array of monopoles $+Q$ and a constant negative charge density $\rho_0=\bar{\rho}_{\text{out}}$. The monopoles are placed at the center of each APW sphere and are of strength

$$\bar{\rho}_{\text{out}}\,\Omega_{\text{cell}}=\textstyle\sum_\nu (+Q) \ . \tag{8}$$

The magnitude of the monopole $(-Q)$ in (7) is identical to that of the monopole $(+Q)$ in (8).

Our final expressions for the muffin-tin potential-energy solutions to the above problems (including the $\chi\alpha$ exchange potential) are

$$V^{\text{in}}(r) = -\frac{2Z_\nu}{r} + \frac{8\pi}{r}\int_0^r \bar{\rho}_{\text{in}}(r)r^2 dr + 8\pi\int_r^{S_\nu} \bar{\rho}_{\text{in}}(r) r\,dr - 6\alpha\left(\frac{3}{8\pi}\,\bar{\rho}_{\text{in}}(r)\right)^{1/3} \tag{9}$$

inside the APW sphere, and

$$V^{\text{out}} = \frac{4\pi S_\nu^2 \bar{\rho}_{\text{out}}}{\Omega_0}\left[\Omega_{\text{cell}}\left(1-\frac{2}{3}\,\frac{b}{a}\,S_\nu\right)+\frac{8\pi}{15}\,S_\nu^3\right] + 4\pi\bar{\rho}_{\text{out}}S_\nu^2 - \bar{\rho}_{\text{out}}\,\frac{b}{a}\,\Omega_{\text{cell}} - 6\alpha\left(\frac{3\bar{\rho}_{\text{out}}}{8\pi}\right)^{1/3} \tag{10}$$

in the region outside. For hcp crystal structure, we determine the constant b in (10) to be

$$b = \frac{2\pi a}{\Omega_{\text{cell}}\,\epsilon^2} + \frac{2\epsilon a}{\pi^{1/2}} - \frac{4\pi a}{\Omega_{\text{cell}}}\sum_{\vec{g}\neq 0}\frac{e^{-g^2/4\epsilon^2}}{g^2}\,(1+e^{i\vec{g}\cdot\vec{\tau}}) - \sum_{\vec{R}'\neq 0}\frac{\operatorname{erfc}\epsilon(\vec{R}')}{|\vec{R}'|/a} \ . \tag{11}$$

This expression is independent of ϵ which is a convergence factor. The quantity a is the "principal" lattice constant (in the case of the hcp crystal structure there are two lattice constants). The expression for b takes into account the nonsymmorphic nature of the space group for the hcp crystal structure by including the phase factor $e^{i\vec{g}\cdot\vec{\tau}}$ in the third term, a factor which is equal to unity for crystals having symmorphic space groups.

These expressions for the potential energy are written such that the constant terms which are found in $V^{\text{in}}(r)$ are shifted to appear in V^{out}. Also, the calculation is performed by setting the average background potential equal to zero in the process of solving the generalized Ewald potential problem, a trick which can be done within the muffin-tin approximation.

The new muffin-tin potential obtained above is averaged with the muffin-tin potential used in the previous iteration in order to speed convergence. The weighting is determined by trial iterations since no clear-cut analytical procedure exists for determining an optimum value for the averaging. Typically only four or five iterations are required to achieve self-consistency, once an optimum weighted average is found.

C. Group Theoretical Analysis

The number of reciprocal-lattice vectors required to obtain reasonably convergent eigenvalues for titanium (to within 0.0025 Ry) produces a rather large secular determinant, typically of the order of at least 30×30. At high-symmetry points and along high-symmetry directions, the determinant can be reduced to a set of appreciably smaller determinants if one uses symmetrized functions which transform irreducibly under the group of the wave vector for the point in question. The crystal structure for titanium is characterized by the D_{6h}^4 nonsymmorphic space group, so that the problem of finding the irreducible representations of the space group is somewhat more complicated. It is no longer possible to deal with representations of the translational group and point group separately.

The operators of the space group are of the form $\{\underline{R}|\vec{\tau}_n+\vec{\tau}_R\}$, where $\vec{\tau}_n$ is a primitive lattice translation and $\vec{\tau}_R$ is equal either to 0 or $\vec{\tau}$ depending on whether or not a nonprimitive translation is necessary after the operation $\underline{R}$. The point group G_0 therefore is no longer a subgroup of the space group G because of the necessity of translating by $\vec{\tau}$ after some of the point group operations.

The problem of finding the irreducible representations of the space group is the same as that for symmorphic space groups in that one seeks the irreducible representations of the group of the wave vector $G(\vec{k}_0)$. However, these representations now satisfy

$$\underline{\Gamma}_\rho(\{E|\vec{t}\}) = e^{i\vec{k}_0\cdot\vec{t}_R}\,\underline{\Gamma}_\rho(\{E|\vec{t}_n\}) \ ,$$

where $\vec{t}=\vec{t}_n+\vec{t}_R$. Furthermore, the effect of operating on a Bloch function $\phi_{\vec{k}_g}(\vec{r})$, using Slater's[16] notation, is

$$\{\underline{R}|\vec{t}\}\phi_{\vec{k}_g}(\vec{r}) = e^{i\vec{k}_0\cdot(\vec{t}_n+\vec{t}_R)}\,e^{i\vec{g}\cdot\vec{t}_R}\,\phi_{\underline{R}^{-1}\vec{k}_g}(\vec{r}) \ .$$

The projection operators[17] used to form sym-

metrized basis functions are of the form

$$P^{p}_{ss}=\frac{l_p}{g(\vec{k}_0)}\sum_{\{\underline{R}|\vec{t}\}}\Gamma^{*}_{p}(\{\underline{R}|\vec{t}\})_{ss}\{\underline{R}|\vec{t}\}\,, \tag{12}$$

where p is the dimension of the pth irreducible representation, $g(\vec{k}_0)$ is the order of the group $G(\vec{k}_0)$, and the summation is over all operations in the group $G(\vec{k}_0)$, including the translations. Because of the differences between representations (and operators) of symmorphic and nonsymmorphic space groups, the projection operator (12) for a nonsymmorphic space group becomes

$$P^{p}_{ss}=\frac{l_p}{g(\vec{k}_0)}\sum_{\{\underline{R}|\vec{t}_R\}}\Gamma^{*}_{p}(\{\underline{R}|\vec{t}_R\})_{ss}\{\underline{R}|\vec{t}_R\}\,, \tag{13}$$

where the summation no longer includes the primitive translations. Just as in the case for symmorphic space groups, the factor $e^{i\vec{k}_0\cdot\vec{t}_n}$ due to $\{\underline{R}|\vec{t}\}$ is cancelled by the phase factor of the complex conjugate of the representation matrix, $\underline{\Gamma}_p(\{\underline{R}|\vec{t}\})$.

A suitable set of symmetrized APW's for reducing the size of the secular determinant therefore is

$$\Phi^{p}_{\vec{k}_g s}=\frac{l_p}{g(\vec{k}_0)}\sum_{\{\underline{R}|\vec{t}_R\}}\Gamma^{*}_{p}(\{\underline{R}|\vec{t}_R\})_{ss}\,e^{i\vec{k}_g\cdot\vec{t}_R}\,\chi_{\underline{R}^{-1}\vec{k}_g}(\vec{r}),$$

$$s=1,\ldots l_p \tag{14}$$

where p ranges over the set of irreducible representations of $G(\vec{k}_0)$. Slater[16] has listed the matrix elements of the irreducible representations for all high-symmetry points and directions of the D^4_{6h} space group. One has only to compute the phase factor $e^{i(\vec{k}_0+\vec{g})\cdot\vec{t}_R}$ for each transformed APW, $\chi_{\underline{R}^{-1}\vec{k}_g}(\vec{r})$ in order to produce a correctly symmetrized APW basis function using Slater's matrix elements. Once the functions (14) have been found, they are used in (2) to represent $\psi_{\vec{k}_0}(\vec{r})$.

Using the set (14) in the expansion (2), the large original determinant (3) is reduced to a product of smaller determinants

$$|D|=\Pi_p\,\Pi_s\,|D(p,s)|\,,$$

where

$$|D(p,s)|=\det|(\Phi^{p}_{\vec{g}s},H\Phi^{p}_{\vec{g}'s})+S\Phi^{p}_{\vec{g}\vec{g}'s}-E(\Phi^{p}_{\vec{g}s},\Phi^{p}_{\vec{g}'s})|\,.$$

The largest reduced determinant occurring in the calculation using 43 reciprocal-lattice vectors is 12×12 with the typical determinant being of the order of 6×6.

III. DETAILS AND RESULTS OF CALCULATION

Titanium is a transition metal with an open d-shell atomic configuration of either $3d^3 4s^1$ or $3d^2 4s^2$, and it has the hcp crystal structure. The unit cell and BZ are shown in Fig. 1. The basis vectors of the direct and reciprocal lattice are given by

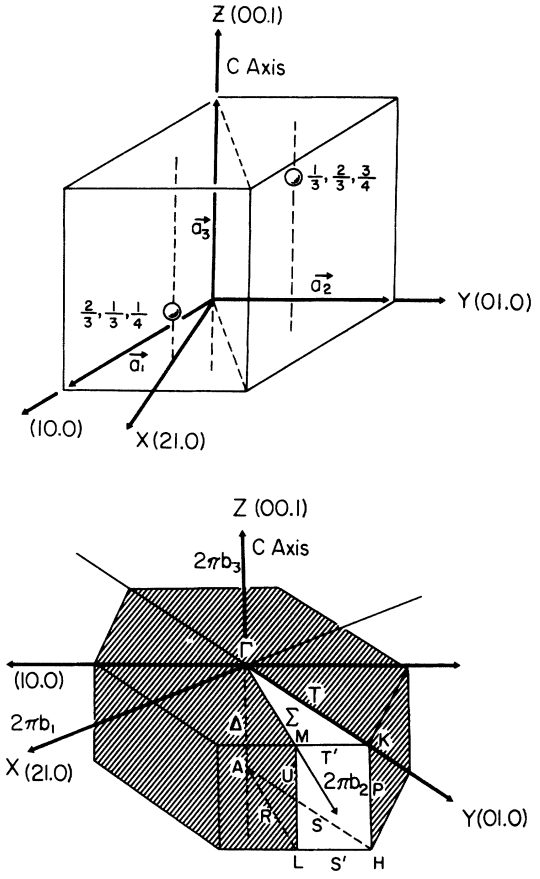

FIG. 1. Unit cell and half of the BZ for the hcp crystal structure with the $\frac{1}{24}$ zone and crystal symmetry directions shown.

$$\vec{a}_1=\tfrac{1}{2}\sqrt{3}\,a\hat{x}-\tfrac{1}{2}a\hat{y},\quad \vec{a}_2=a\hat{y},\quad \vec{a}_3=c\hat{z}$$

and

$$\vec{b}_1=(2/\sqrt{3}a)\,\hat{x},\quad \vec{b}_2=(1/\sqrt{3}a)\,\hat{x}+(1/a)\,\hat{y},\quad \vec{b}_3=(1/c)\,\hat{z}\,.$$

The lattice constants are $a=5.576\,897$ a.u. and $c=8.885\,227$ a.u., giving a ratio of $c/a=1.587\,31$ as compared to the perfect hcp crystal structure for which $c/a=(\frac{8}{3})^{1/2}=1.632\,99$. The basic dimensions of the BZ therefore are $\Gamma A=0.650$ (a.u.)$^{-1}$, $\Gamma K=0.751$ (a.u.)$^{-1}$, $\Gamma M=0.650$ (a.u.)$^{-1}$, and $MK=0.376$ (a.u.)$^{-1}$. The reciprocal-lattice vectors used in the APW expansion are designated by

$$\vec{g}=(n_1,n_2,n_3)=2\pi(n_1\vec{b}_1+n_2\vec{b}_2+n_3\vec{b}_3)\,.$$

For our choice of unit cell, the nonprimitive translation is $\vec{\tau}=\frac{1}{2}c\hat{z}$ and the phase factor which occurs in the symmetrized APW's is given by

$$e^{i(\vec{k}_0+\vec{g})\cdot\vec{\tau}}=e^{i(k_{0z}c/2+n_3\pi)}\,. \tag{15}$$

The constant b was calculated using an optimum

TABLE I. The 43 reciprocal-lattice vectors used in part in the APW expansions at high-symmetry points.

		$(\bar{1}12)$	$(\bar{1}02)$	$(0\bar{1}2)$	(002)	(012)	(102)	$(1\bar{1}2)$			
		$(\bar{1}11)$	$(\bar{1}01)$	$(0\bar{1}1)$	(001)	(011)	(101)	$(1\bar{1}1)$	$(1\bar{2}1)$		
$(0\bar{2}0)$	$(\bar{1}\bar{1}0)$	$(\bar{1}10)$	$(\bar{1}00)$	$(0\bar{1}0)$	(000)	(010)	(100)	$(1\bar{1}0)$	$(1\bar{2}0)$	$(2\bar{1}0)$	$(2\bar{2}0)$
		$(\bar{1}1\bar{1})$	$(\bar{1}0\bar{1})$	$(0\bar{1}\bar{1})$	$(00\bar{1})$	$(01\bar{1})$	$(10\bar{1})$	$(1\bar{1}\bar{1})$	$(1\bar{2}\bar{1})$		
		$(\bar{1}1\bar{2})$	$(\bar{1}0\bar{2})$	$(0\bar{1}\bar{2})$	$(00\bar{2})$	$(01\bar{2})$	$(10\bar{2})$	$(1\bar{1}\bar{2})$			
					$(00\bar{3})$						

value of $\epsilon = 2.8a$ with the result $b = 3.272\,27$. A check of our expression was made by calculating b for the fcc structure. Our value $b = 4.584\,87$ compares well with a value $b = 4.584\,86$ reported by Connolly.[18] Finally, the APW sphere radius used was $S_v = 2.718$ a.u.

A. Convergence Studies

The set of reciprocal-lattice vectors listed in Table I were used in the APW expansion and gave an energy convergence good to within 0.0025 Ry based on a study made at the high-symmetry points in the BZ.

Both the APW matrix elements (3) and the iterated crystal charge density $\bar{\rho}_{in}(r)$ contain an infinite sum on l. In this calculation the sum has been truncated at $l = 6$ with no loss in energy convergence: At symmetry point Γ the energy eigenvalues for $l = 6$ were within 0.001 Ry of those calculated using $l = 10$ for both the initial calculation and the first iteration.

For this calculation, we have chosen the more accepted atomic configuration $3d^2 4s^2$, and the atomic charge densities used to initiate the self-consistent-field calculation were those of Liberman.[19] The charge densities and corresponding contribution to the muffin-tin potential acquired from the core atomic orbitals were assumed to remain atomiclike and were not included in the iteration process. This assumption was presumed valid only for orbitals whose charge density is essentially contained within the APW sphere. For the titanium core orbitals used, 99.7% of the charge lies within the APW sphere. In contrast, only ~85% of the $3d$ atomic charge density and 54% of the $4s$ atomic charge density are contained within the APW sphere. Evidently, the $3d$-band orbitals have considerable atomic character while the $4s$-band orbitals should be very plane-wave-like. Because of the partially filled d bands in titanium the true crystal potential has a highly nonspherical component within the APW spheres so that our muffin-tin calculation can be considered to yield only a zero-order approximation in this sense to the "true" Fermi surface and energy bands.

Titanium has 22 electrons for the neutral atom. The charge density used in the iterative process therefore consisted only of $\bar{\rho}_{in}(r)$ and $\bar{\rho}_{out}$, due to the outer 4 electrons, which was calculated by a weighted sum over Bloch states as described in Sec. II B. The muffin-tin potential due to the remaining 18 electrons was obtained using atomic densities in the method described by Mattheiss[14] and was held fixed. This was added to the iterated potential generated by $\bar{\rho}_{in}(r)$ and $\bar{\rho}_{out}$ to form the new iterated muffin-tin potential. Clearly, the core charge density is incorrectly described since it is not acquired from Bloch functions which are orthogonal to the valence electron wave functions described by combinations of our symmetrized APW's. However, for titanium, the description should be adequate since the atomic potential is approximated quite well by the muffin-tin potential in the region occupied by the core electrons.

B. Self-Consistency Convergence Studies

Before presenting the results acquired using our self-consistent muffin-tin potential, we discuss some specific problems associated with obtaining rapid convergence to self-consistency. In order

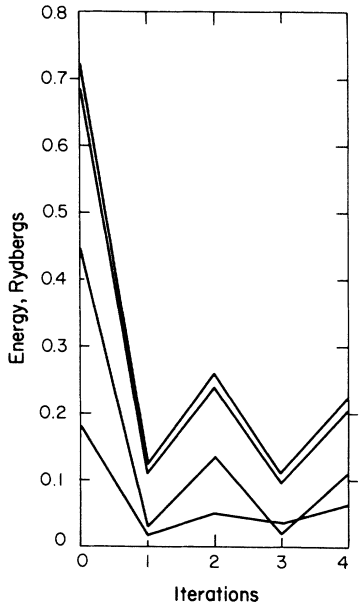

FIG. 2. Slow convergence of energy eigenvalues at the Γ point in the iteration procedure using $\beta = 1$ and $\alpha = \frac{3}{4}$.

TABLE II. High symmetry used in the iteration process.

Point	Coordinates $\hat{x}\left(\frac{2\pi}{a}\right)$	$\hat{y}\left(\frac{2\pi}{a}\right)$	$\hat{z}\left(\frac{2\pi}{c}\right)$	Number of vectors in "star of $\vec{k}$"
Γ^*	0	0	0	1
A^*	0	0	$\frac{1}{2}$	1
Δ	0	0	$\frac{1}{4}$	2
K^*	0	$\frac{2}{3}$	0	2
H^*	0	$\frac{2}{3}$	$\frac{1}{2}$	2
M^*	$1/\sqrt{3}$	0	0	3
L^*	$1/\sqrt{3}$	0	$\frac{1}{2}$	3
T	0	$\frac{1}{3}$	0	6
Σ	$1/2\sqrt{3}$		0	6
R	$1/\sqrt{3}$	0	$\frac{1}{4}$	6
P	0	$\frac{2}{3}$	$\frac{1}{4}$	12
U	$1/\sqrt{3}$	0	$\frac{1}{4}$	12
S	0	$\frac{1}{3}$	$\frac{1}{2}$	6
S'^*	$1/\sqrt{3}$	$\frac{1}{6}$	$\frac{1}{2}$	12
T'^*	$1/\sqrt{3}$	$\frac{1}{6}$	0	12
T^*	0	$\frac{2}{9}$	0	6
T^*	0	$\frac{4}{9}$	0	6
Σ^*	$1/3\sqrt{3}$	0	0	6
Σ^*	$2/3\sqrt{3}$	0	0	6
R^*	0	$\frac{2}{9}$	$\frac{1}{2}$	6
R^*	0	$\frac{4}{9}$	$\frac{1}{2}$	6
S^*	$1/3\sqrt{3}$	0	$\frac{1}{2}$	6
S^*	$2/3\sqrt{3}$	0	$\frac{1}{2}$	6
P^*	0	$\frac{2}{3}$	$\frac{1}{6}$	12
P^*	0	$\frac{2}{3}$	$\frac{1}{3}$	12
U^*	$1/\sqrt{3}$	0	$\frac{1}{6}$	12
U^*	$1/\sqrt{3}$	0	$\frac{1}{3}$	12
Δ^*	0	0	$\frac{1}{3}$	2
Δ^*	0	0	$\frac{1}{6}$	2

to speed convergence, the potential (rather than the charge density) was averaged from one iteration to the next. The averaged potential is expressed

$$V_{\text{av}} = \beta V' + (1-\beta)V, \quad 0 \leq \beta \leq 1 . \tag{16}$$

Here V' is the potential from a given iteration and V is that from the previous iteration. An example of the effect on the eigenvalues at the Γ point of the choice of β is shown in Figs. 2 and 3. For both these cases, the following high-symmetry points

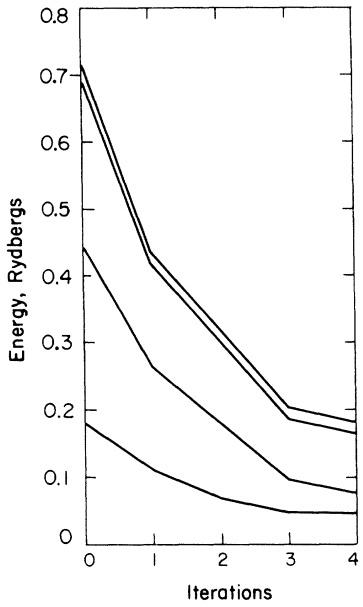

FIG. 3. Slow convergence of energy eigenvalues at the Γ point in the iteration procedure using $\beta = \frac{1}{2}$ and $\alpha = \frac{3}{4}$.

were used (see Fig. 1 and Table II) to obtain a muffin-tin charge density: $\Gamma, \Delta, A, K, M, L$, and H, a sampling equivalent to 14 points in the BZ. Also, they were performed using $\frac{3}{4}$ of the Slater exchange potential (a value ultimately used in the final calculation).

Figure 2 shows the results of the first four iterations with no averaging ($\beta = 1$) for succeeding itera-

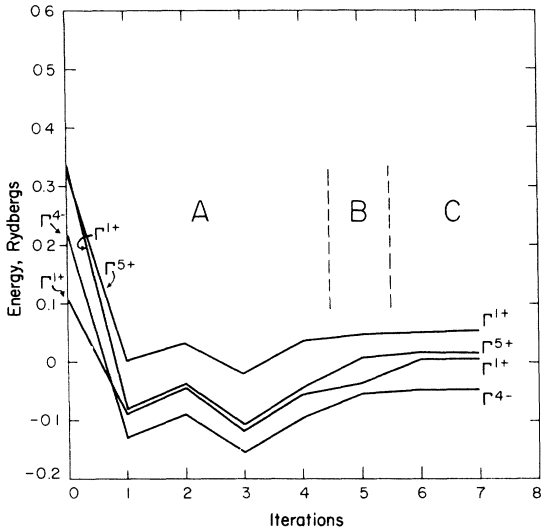

FIG. 4. Energy convergence to self-consistency in the iteration procedure using $\beta = \frac{1}{2}$ and $\alpha = 1$ which gives flipping of s and d bands.

tions. Convergence is extremely slow as evidenced by the strong oscillation in eigenvalues from one iteration to the next. Figure 3 shows the results for the first four iterations using equal weighting ($\beta = \frac{1}{2}$) between the new and old potentials. Convergence is also slow for this case since the eigenvalues continue to change monotonically by a significant percentage from one iteration to the next. Ultimately a value of $\beta = 0.65$ was found to give optimum convergence to self-consistency for titanium.

C. Choice of Exchange Approximation

Next, a study was made to determine the effect of various choices of α in the $\chi\alpha$ approximation to the exchange potential. Figure 4 shows the results of seven iterations for a potential using full ($\alpha = 1$) Slater exchange and $\beta = \frac{1}{2}$ averaging. The first four iterations labeled *A* were performed using the seven high-symmetry points listed above. The fifth iteration labeled *B* included two additional points, *T* and Σ, while the last two iterations labeled *C* were performed using the first twelve high-symmetry points listed in Table II. Including points *R*, *P*, and *U* to those already mentioned gave a sampling of the BZ at 56 points. The eigenvalues have converged with the *d* band shifted below the *s* band, a result which most likely is nonphysical. Also, the bandwidth is considerably narrower than in our previously reported results.

A second choice, $\alpha = \frac{5}{6}$, $\beta = 0.7$, gave the results shown in Fig. 5. Once again the flipping of the *s* and *d* bands and the narrowing of the bandwidth occurs. This calculation was not carried to self-consistency since the pattern established indicated results similar to those for the full Slater exchange.

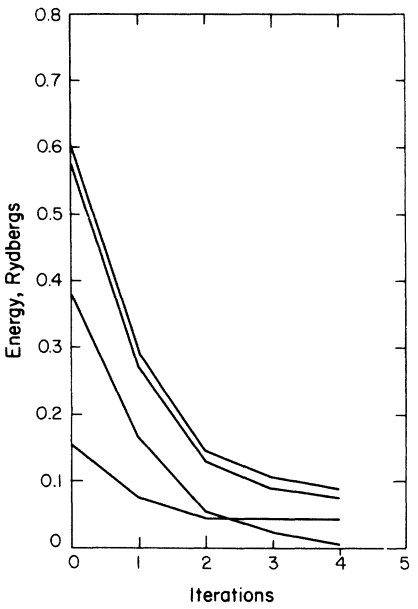

FIG. 5. Energy convergence at the Γ point in the iteration procedure using $\beta = 0.7$ and $\alpha = \frac{5}{6}$ which gives flipping of *s* and *d* bands.

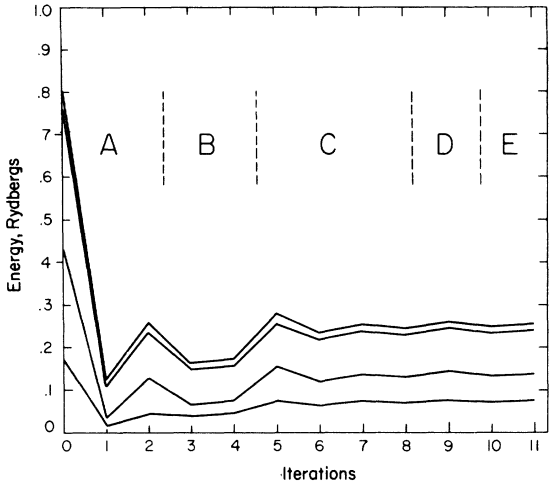

FIG. 6. Energy convergence to self-consistency at the Γ point in the iteration procedure using $\beta = 0.65$ and $\alpha = \frac{3}{4}$.

Finally, a convergence study for the choice $\alpha = \frac{3}{4}$, $\beta = 0.65$ was made at the Γ point with the results shown in Fig. 6. The first two iterations labeled *A* included only the Γ point charge density and used the entire new potential ($\beta = 1$). The third through the eleventh iterations were performed using $\beta = 0.65$. The third and fourth iteration labeled *B* include the first seven high-symmetry points listed in Table II. The fifth through eighth iteration labeled *C* use the first twelve high-symmetry points. Relative convergence has been obtained. As a check, the next three high-symmetry points were added and a ninth iteration labeled *D* was performed. Enough change occurred that two more iterations labeled *E* were carried out using the 22 high-symmetry points marked with asterisks in Table II, a set of points equivalent to a 136-point sampling of the BZ.

This study was made to determine convergence with respect to the size of the sampling mesh as well as convergence to a set of results indicative of the choice of the Slater exchange. Very little relative change in the eigenvalues occurred between the eighth and eleventh iterations in which 80 additional high-symmetry points have been added to the sampling used to determine the muffin-tin charge density. For this choice of α, the ordering of the *s* and *d* bands is unchanged and the bandwidth is essentially the same as that obtained in HW (I).

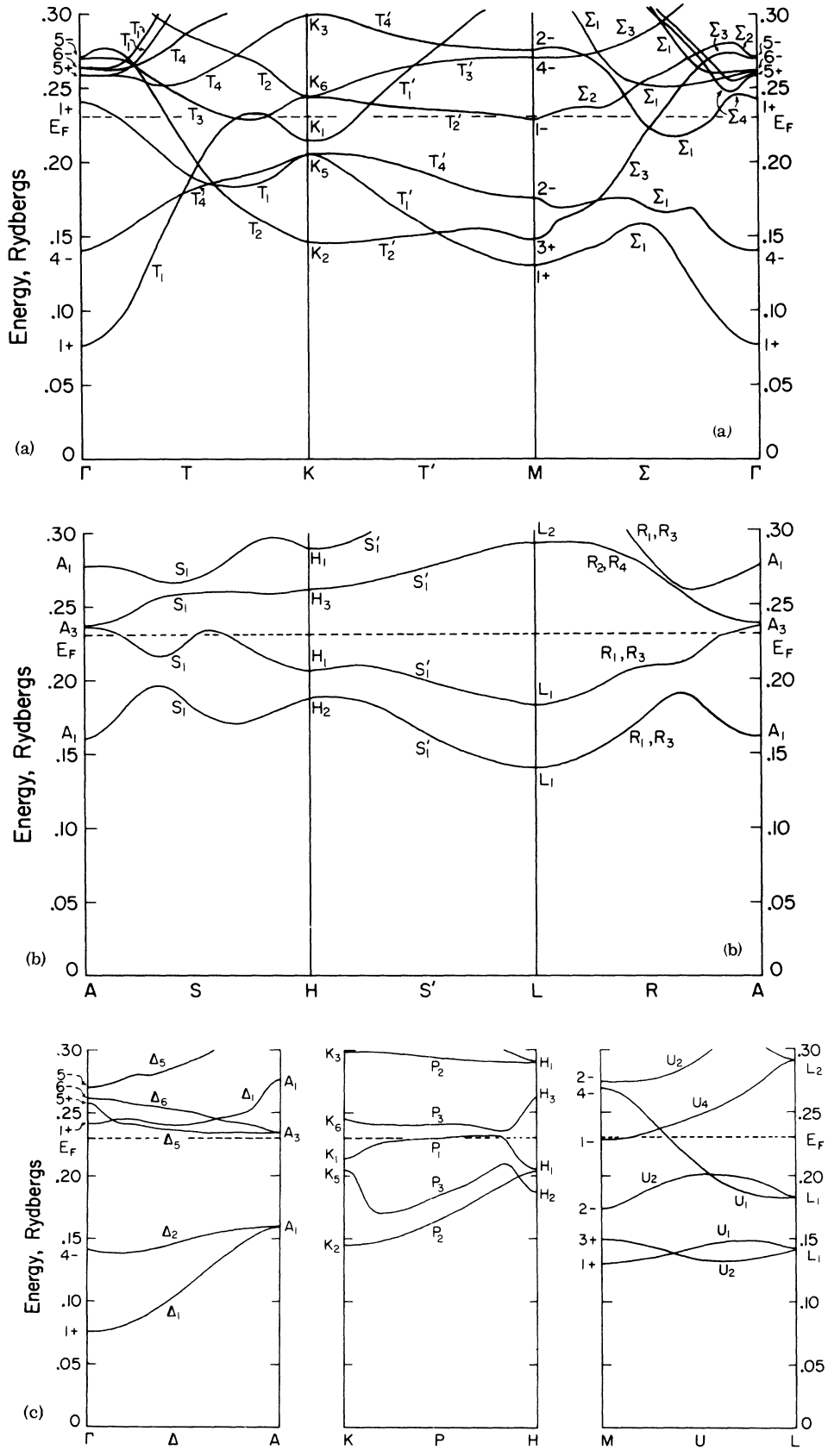

FIG. 7. Energy bands of titanium along symmetry directions acquired with the self-consistent muffin-tin potential. All levels in 7(b) are doubly degenerate.

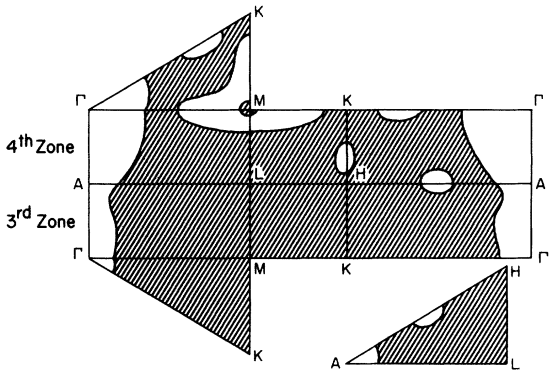

FIG. 8. Intersections of the Fermi surface with the symmetry planes of the $\frac{1}{24}$ double-zone wedge for the third and fourth zone.

D. Band Structure and Fermi Surface

Using the self-consistent muffin-tin potential calculated with the choice $\alpha = \frac{3}{4}$, the energy bands and Fermi surface were calculated in the same manner as described in HW (I). The computations were carried out over a discrete mesh equivalent to 3024 points in the BZ. The eigenvalues were found at 126 general points in the $\frac{1}{24}$ zone shown in Fig. 1 using the scheme described in HW (I); and they were computed for all high-symmetry points and along high-symmetry directions. The Fermi energy was found by arranging in increasing value the 126 sets of eigenvalues in the $\frac{1}{24}$ zone. Since there are four valence electrons per atom and two atoms per unit cell (see Fig. 1), there are eight electrons per unit cell to be accommodated. Each band can accommodate two electrons per cell (spin up and spin down) so that there exist four full bands on the average. Thus, $(8 \div 2) \times 126 = 504$ lowest-energy eigenstates are occupied, and the Fermi energy accurate to one part in 504 is given

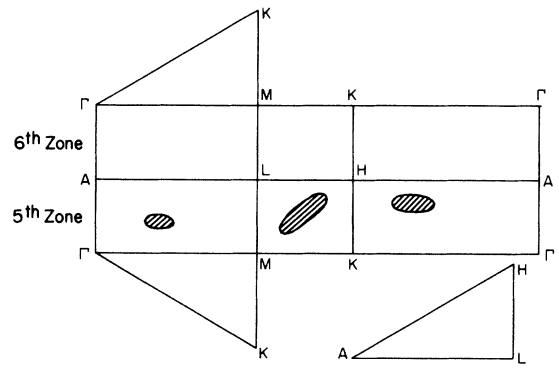

FIG. 9. Intersections of the Fermi surface with the symmetry planes of the $\frac{1}{24}$ double-zone wedge for the fifth and sixth zone.

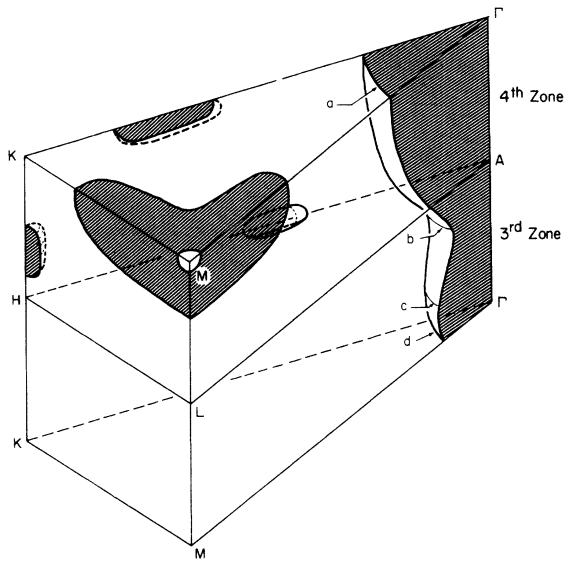

FIG. 10. Basic Fermi-surface portions for the third and fourth zone. Some of the possible electron orbits are labeled with lower case Roman letters.

by that of the highest occupied energy state. The highest occupied state was found to have $E_F = 0.230$ Ry. The energy of the lowest state at Γ was 0.077 Ry, which gives an occupied bandwidth of 0.153 Ry. This is smaller than the value 0.211 Ry found in HW (I), and it suggests that a smaller exchange contribution (say $\alpha < \frac{3}{4}$) may be more appropriate.[20] Since no experimental data exist, to which a reasonable fit can be made, the question of a choice of α remains open.

The energy bands along high-symmetry directions are shown in Fig. 7. Once again, the double-zone scheme is used to display connections of the Fermi surface in the third and fourth as well as fifth and sixth zones. The intersection of the Fermi surface with the $\frac{1}{24}$ zone wedge for the third and fourth zone is shown in Fig. 8 and that for the fifth and sixth zone is shown in Fig. 9. Each figure actually displays intersections with the double-zone wedge with the triangle showing intersection with the *ALH* symmetry plane. The shaded parts of both figures are electron occupied. The Fermi surface in the double-zone scheme is shown in Figs. 10 and 11.

E. Density of States

The determination of the Fermi energy provides a means of constructing a density-of-states histogram. The results of the counting scheme are shown in Fig. 12. The typical density-of-states curve for hcp metals is exhibited in this case. There are two peaks due to the narrow *d* bands with the Fermi energy occurring on the high-energy side

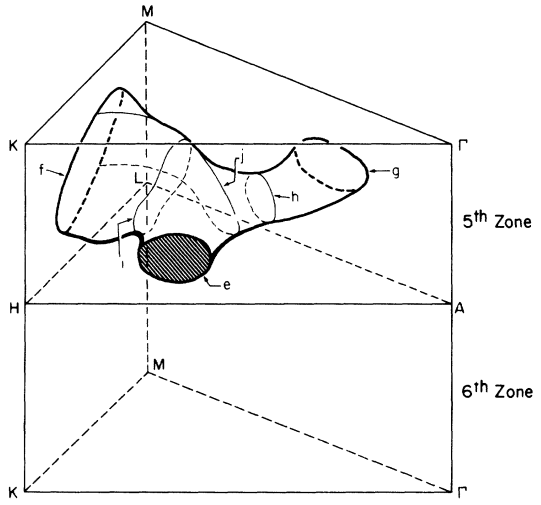

FIG. 11. Basic Fermi-surface portion for the fifth and sixth zone. Possible electron orbits are labeled with lower case Roman letters.

of the second peak. At the Fermi energy, the density of states is 22.0 electrons per atom per Ry, which gives an electronic specific-heat coefficient of $\gamma = 4.31$ mJ mole^{-1} deg^{-2} (9.13×10^{-4} cal mole^{-1} deg^{-2}). This compares well with the result 11.8×10^{-4} cal mole^{-1} deg^{-2} obtained in HW (I). Experimental results are 8.0×10^{-4} cal mole^{-1} deg^{-2} obtained by Daunt[7] and 3.41 ± 0.10 mJ mole^{-1} deg^{-2} quoted by Gschneider.[8] Once again, our result most likely is high because of the course determination of the Fermi energy and the density of states at the Fermi energy.

Our density-of-states histogram indicates a d-band width at half-maximum of ~0.08 Ry or ~1.1 eV. Like the results for occupied bandwidth, this is narrower than the value predicted in HW (I). A recent photoemission study of titanium by Eastman[5] shows that the width at half-maximum is ~2.0 eV. Weiss[6] has determined the density of states by Compton scattering, and his outer limit for the d-band width is ~4 eV. Both of these results are considerably larger than our prediction, thus suggesting that our choice of exchange parameter ($\alpha = \frac{3}{4}$) is too large.

IV. DISCUSSION

A. Comparison with Other Papers

The energy bands shown in Fig. 7 are almost identical with those obtained in HW (I), but with some notable differences. They are similar to the Ti^{+4} structure of AB but with too many notable differences to make a meaningful comparison. With the use of group theory we were able to label each state according to symmetry and thus resolve the question of continuity of the energy solutions as we trace them out from one high-symmetry point to another. This was not done in HW (I). The low-energy symmetry band T_1 between Γ^{1+} and K_1 is now shown to cross the Fermi level, and the structure along ΓMK is more clearly defined than in HW (I). The fifth band no longer dips below the Fermi level along KM or along ΓK so that the structure in the fifth and sixth zone is significantly altered. The same general features along $AHLA$ occur as in HW (I) except that the third and fourth bands cross the Fermi level along AH and the fifth and sixth bands no longer dip below the Fermi level along AH. The structure along ΓA is essentially the same except for slight differences for the structure above the Fermi level. Along KH however, the structure is quite different from that in HW (I), and the symmetry band P_1 is now observed to cross the Fermi level. The structure along ML, close to M, is somewhat different from that in HW (I), but it retains the same number of crossings of the Fermi level.

The Fermi surfaces provide for a more definitive comparison among the calculations. The third- and fourth-zone surfaces (see Figs. 8 and 10) along $\Gamma A\Gamma$ are quite similar to those of HW (I) except that the minimum in the third zone now occurs at about $0.75\Gamma A$ rather than in the AHL plane, and the structure near Γ in the fourth zone is much smoother. The indentations in the surface at Γ shown in HW (I) are quite likely due to ambiguities in assigning band labels to the results. The fourth-zone surfaces around the point M are essentially the

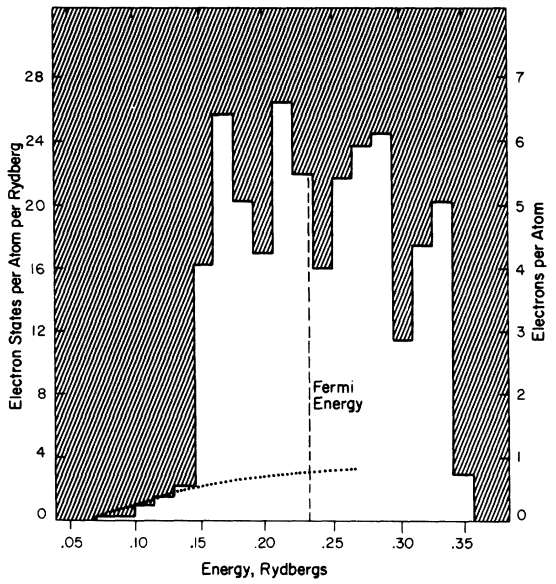

FIG. 12. Histogram of the density of states with the Fermi energy indicated by a dashed line. The dotted curve is from the free-electron model.

same as those of HW (I), except that the electron pocket is considerably smaller. The notable exceptions are the three pockets of holes along ΓK, AH, and KH which are not present in the work of AB or in HW(I). A comparison with the calculations of AB shows that the gradual evolution of their model with increased valency could produce our third- and fourth-zone results if they had increased the potential even more.

The fifth- and sixth-zone surface shows more similarities than differences when compared to that of HW (I), and it bears little resemblance to the results of AB. The multiply connected electron surface, shown in Figs. 9 and 11, differs from that of HW (I) only in the following respects: (i) The present results indicate no electron structure in the sixth zone at all and, in particular, no surface extending into the sixth zone along AH; (ii) the surface does not contact the ΓKM plane or the ΓAHK plane along ΓK in the fifth zone; and (iii) the surface contacts the $KHLM$ plane without intersecting the line KM. In spite of these differences, the major features are preserved. The intersections of the electron surface with the ΓALM, ΓAHK, and $KHLM$ planes still occur, and the multiply connected toruslike surfaces around the vertical axes ΓA and KH are present.

B. de Haas–van Alphen Periods

The third- and fourth-zone surface along $\Gamma A\Gamma$ clearly gives four extremal cross sections normal to the c axis or [00.1] direction. We again use the dot notation $[a_1 a_2 \cdot c]$ discussed in HW (I), but we point out that the labeling in HW (I) should have been $[a_2 a_3 \cdot c]$. Portions of the corresponding orbits are labeled a, b, c, and d in Fig. 10. The periods, in units of $10^{-8}(\mathrm{GHz})^{-1}$, are given in Table III. The four easily observable periods of these four orbits will vary with angle and eventually become unmeasurable for angles above approximately 30°.

TABLE III. Periods of the orbits labeled in Figs. 10 and 11.

Direction	Orbit		Period $[10^{-3}(\mathrm{GHz})^{-1}]$
[00.1]	Third and fourth bands	a(hole)	1.4
		b(hole)	10.0
		c(hole)	4.1
		d(hole	6.0
[01.0]	Fifth and sixth bands	g(elec.)	56.5
		h(elec.)	74.0
[$\bar{1}$1.0]	Fifth and sixth bands	e(elec.)	27.0
		f(elec.)	10.8
		i(elec.)	32.5
		J(elec.)	5.4

The fourth-zone hole and electron surfaces at M give two sets of periods which are essentially the same for the applied field along the directions [00.1], [10.0], and [$\bar{1}$1.0] [i.e., along ΓA, ΓK (or MK), and ΓM, respectively]. The cross sections centered on M give the following periods for holes:

	direction	period $[10^{-8}(\mathrm{GHz})^{-1}]$
	[00.1]	1.87
M:(hole)	[10.0]	3.15
	[$\bar{1}$1.0]	1.50

and the following periods for electrons:

	direction	period $[10^{-8}(\mathrm{GHz})^{-1}]$
	[00.1]	83.5
M:(electron)	[10.0]	74.0
	[$\bar{1}$1.0]	67.0

The electron orbits, with their very long periods, are excellent candidates for low-field study provided pure enough crystals are available.

The pockets of holes along ΓK, AH, and KH produce periods as follows:

	direction	period $[10^{-8}(\mathrm{GHz})^{-1}]$
	[00.1]	18.5
ΓK:(hole)	[10.0]	44.5
	[$\bar{1}$1.0]	14.2
	[00.1]	24.2
AH:(hole)	[10.0]	57.0
	[$\bar{1}$1.0]	22.3
	[00.1]	43.0
KH:(hole)	[10.0]	18.0
	[$\bar{1}$1.0]	17.1

These surfaces (like the electron surface at M) have large periods which would be difficult to measure unless reasonably pure single crystals were available. The ΓK and AH surfaces have periods which change rapidly with angular variation about the [10.0] direction, whereas the KH surface has periods which change rapidly with angular variations about the [00.1] direction.

The periods for orbits associated with the multiply connected fifth-zone electron surface are listed in Table III. The orbits labeled e, f, g, h and i are closed orbits within the $\frac{1}{24}$ double-zone wedge. In contrast, the orbit labeled j is displayed only in part (see Fig. 11). The diagram shows that all of these orbits are extremely sensitive to angular variation due to the topography of the Fermi surface. Also, most all have periods which are quite large so that once again pure single crystals are required.

V. CONCLUSIONS

The fact that no experimental Fermi-surface data exists leaves doubt as to the theoretical predictions given by AB and by the authors here and in HW (I). The choice of the exchange potential parameter used in the present calculation is smaller than the value $\alpha = \frac{5}{6}$ used by Snow[21] in his best calculation of the electronic structure of copper. We find a shifting of the d band below the s band for both the $\alpha = 1$ and $\alpha = \frac{5}{6}$ Slater-exchange potential, a feature not given by Snow's calculation. Copper of course is a closed d-shell nearly-free-electron-like metal whereas, titanium is an open d-shell transition metal. We realize that the nonspherical atomiclike flavor of the d-band orbitals is not accounted for by the muffin-tin charge density and potential approximation. Also, in a case such as this, the choice of the same exchange potential parameter for all bands may not be the best choice.

We find the same narrowing of the bands and density-of-states histogram for the large values of α as did Snow. We felt that the value $\alpha = \frac{3}{4}$ constituted a reasonable choice for a titanium energy band calculation,[20] but the results suggest that it is too large. The choice $\alpha = \frac{2}{3}$ typically has given incorrect fits for band calculations[21] even though it is shown to be correct[22,23] for an interacting electron gas. Thus, a value between $\frac{3}{4}$ and $\frac{2}{3}$ is most likely the best. It would be of interest to see whether or not the other transition metals in this period (e.g., zirconium) also display this sensitivity to choice of the exchange potential. In particular, it would be of interest to know whether or not the flipping of the s and d bands is physically correct for the open d-shell metals in this region of the Periodic Table.

ACKNOWLEDGMENTS

The authors would like to thank Dr. David A. Liberman for providing his Hartree-Fock-Slater SCF atomic calculations for titanium. Special thanks are due Miss B. Schwenn for long hours spent plotting the energy bands and drawing the figures. One of us (E. H. H.) is particularly grateful to Dr. Karlheinz Schwartz for an encouraging discussion concerning the choices of exchange potential for band calculations.

---

†Supported by National Science Foundation Grant No. GP-11215.

*Based in part on a thesis submitted to the Physics Department, University of Utah in partial fulfillment of the requirements for a Ph.D. degree.

‡Present address: Department of Geophysics, University of Utah, Salt Lake City, Utah 84112.

[1]L. F. Mattheiss, Phys. Rev. 133, A1399 (1964).

[2]E. H. Hygh and Ronald M. Welch, Phys. Rev. B 1, 2424 (1970).

[3]J. C. Slater, T. M. Wilson, and H. H. Wood, Phys. Rev. 179, 28 (1969).

[4]J. C. Slater, Phys. Rev. 51, 846 (1937).

[5]D. E. Eastman, Solid State Commun. 7, 1697 (1969).

[6]R. J. Weiss, Phys. Rev. Letters 24, 883 (1970).

[7]J. G. Daunt, *Progress in Low Temperature Physics* (North-Holland, Amsterdam, 1955).

[8]K. A. Gschneider, Solid State Phys. 16, 275 (1964).

[9]S. L. Altmann and C. J. Bradley, Proc. Phys. Soc. (London) 92, 764 (1967); Phys. Rev. 135, A1253 (1964).

[10]J. C. Slater, Phys. Rev. 45, 794 (1934).

[11]S. L. Altmann, Proc. Roy. Soc. (London) A244, 141 (1958); A244, 153 (1958).

[12]T. L. Loucks, *Augmented Plane Wave Method* (Benjamin, New York, 1967).

[13]H. Schlosser and P. M. Marcus, Phys. Rev. 131, 2529 (1963).

[14]L. F. Mattheiss, Phys. Rev. 134, A970 (1964).

[15]William E. Rudge, Phys. Rev. 181, 1020 (1969); 181, 1024 (1969); 181, 1033 (1969).

[16]J. C. Slater, *Quantum Theory of Molecules and Solids* (McGraw-Hill, New York, 1965), Vol. 2, Chap. 2.

[17]J. C. Cornwell, *Group Theory and Electronic Energy Bands in Solids* (Wiley, New York, 1969).

[18]J. W. D. Connolly, Ph.D. thesis (University of Florida, 1967) (unpublished).

[19]David A. Liberman Phys. Rev. 159, 415 (1967).

[20]Karlheinz Schwarz, University of Florida, Quantum Theory Project, Report No. 208, 1970 (unpublished); and private communication.

[21]E. C. Snow, Phys. Rev. 171, 785 (1968).

[22]R. Gaspar, Acta Phys. Acad. Sci. Hung. 3, 385 (1954).

[23]W. Kohn and L. J. Sham, Phys. Rev. 140, A1133 (1965).